INTERNATIONAL JOURNAL OF AUTOMOTIVE AND MECHANICAL ENGINEERING (IJAME)
ISSN: 2229-8649 e-ISSN: 2180-1606
VOL. 19, ISSUE 1, 9433 – 9446
DOI: https://doi.org/10.15282/ijame.19.1.2022.07.0726

ORIGINAL ARTICLE

Evaluation of Double-Sided Plasma Vortex Generator in Comparison with Vane Vortex Generator on Separation Control

A.N.M.M.I. Mukut[1,*], H.M.M. Afroz[1], H. Mizunuma[2] and H. Obara[2]

[1]Department of Mechanical Engineering, Dhaka University of Engineering and Technology, Gazipur, Gazipur-1707, Bangladesh
[2]Department of Mechanical Engineering, Tokyo Metropolitan University, 1-1 Minami-Osawa, Hachioji-Shi, 192-0397 Tokyo, Japan

ABSTRACT – The present research has introduced a new type of Plasma Vortex Generator named as Double-Sided Plasma Vortex Generator (DSPVG) that has dual expose electrodes on both sides. This DSPVG is placed normal to the surface parallel to incoming air and creates vortices on it's both sides. As conventional VG has an angle with flow direction which introduce device drag, to overcome this, DSPVG is placed with zero angle with flow direction; besides due to the smaller thickness and frontal area with incoming air than VGs, the drag penalty due to its geometry is minimised. Furthermore, as vortices are created on both sides, DSPVG is expected to reduce the number of Plasma Vortex Generator (PVG) with respect to the conventional embedded PVGs or VGs on the flow controlling surface. Hence, it is able to take advantage of height like conventional VGs and active control systems of PVGs with dual vortices on both sides. The impact of DSPVG on separation control has been investigated experimentally and compared its effectiveness with conventional vane VGs. Three different types of flow measurement techniques have been used to confirm the repeatability and consistency of the experimental results. Numerical investigations have been carried out to evaluate the experimental results. These findings show that the DSPVG is capable to eliminate the separation similarly to the conventional VGs but with higher momentum injection and more effective in minimizing drag penalty in the uncontrolled case as in OFF condition of DSPVG, there is no alternation of local flow which is generally affected in case of VGs that adds drag penalty.

ARTICLE HISTORY
Received: 3rd Aug 2021
Revised: 6th Dec 2021
Accepted: 28th Feb 2022

KEYWORDS
Flow control;
Plasma vortex generator;
Separation control;
Vortex generator;
CFD

INTRODUCTION

Flow separation is a basic flow phenomenon and influences the performance of practical applications. A vortex generator is one of the effective devices for separation suppression. Various types of vortex generators have been found effective in controlling separation in a turbulent boundary layer [1]. Vortex generators have many degrees of freedom in the form of geometrical parameters such as vane shape, height, length and angle to a free stream as well as the chord wise location and spanwise spacing. The performance of vortex generators to mitigate shock-induced separation and their studies is ranging from those conducted in the early post-war era to those performed recently is reviewed in detail [2]. In addition to an airfoil flow, the vortex generators are also used in non-airfoil flows including an internal flow [3], reducing vehicle drag [4]. These vortex generators are installed with an angle to a free stream and produce a parasitic penalty that increases flow resistance. This penalty is critical if the necessary separation control is limited to a temporal short time. A conventional vane-type vortex generator has a height of the order of a boundary layer thickness. In order to minimize the drag penalty, low-profile vortex generators submerged in a boundary layer were developed to control separation [5-7]. On the other hand, plasma vortex generator (PVG) has been developed which consisted of a pair of single dielectric barrier discharge (DBD) plasma actuators embedded in the wall and induced stream-wise counter-rotating or co-rotating vortices like vortex generators and has the ability to control separation in a boundary layer flow [6-11].

The formation mechanism of streamwise vortices by these embedded PVGs was also experimentally investigated [12-14]. It is also found that lift enhancement is obtained by controlling separation in an airfoil [15-17]. A streamwise-oriented DBD vortex generator with and without a boundary layer bleed slot has been investigated and found that those vortex generators led to more robust separation control in adverse pressure gradient configurations [18]. The plasma vortex generator has also been used to suppress the vortex shedding from a train pantograph head [19] and drag reduction has been obtained [20-24]. A normal single plasma actuator is also a useful device to suppress flow separation because a plasma actuator induces a thin jet along the wall and imparts a considerable amount of energy to a boundary layer. Vortex generators, by contrast, induce streamwise vortices, which enhance the mixing between slow near-wall flow and fast outer layer flow in a boundary layer. In this regard, to apply plasma actuator as vortex generator it is necessary to place PVG parallel with the incoming flow so that the induced jet is directed toward the spanwise direction. Hence the induced flow become twisted into the streamwise flow and create vortices as like as conventional VGs. These vortices introduce momentum towards downsteam which is the main mechanism of flow control by embedded PVGs. Thus, the mechanism of separation elimination is different between the normal plasma actuator and the plasma vortex generator (PVG). These

*CORRESPONDING AUTHOR | A.N.M.M.I. Mukut | ✉ mukut@duet.ac.bd

PVGs are embedded on the surfaces in several orientation to create clockwise or counterclockwise vortices as per flow control requirement, but the effectiveness and strength of vorticess is the function of it's geometry, electrode spacing, voltage and frequences. Inadequete spacing of embedded PVGs interfare the adjacent vortices that narrow the effectiveness to attain desired flow control. Moreover, if the boundary layer is thicker the influence of vortices to inject momentum in separated region become limitted due to the embeddedness of PVGs on aerodyanic surface [25-26]. These make the embedded VG's incapable to take advantages of device height which would enhance mixing in separated zone for thicker boundary layer. VG height adds device/parasite drag due to increase frontal area that drastically affect aerodynamic control [27-30], if this drag is neglected, higher the device height of VGs enhance the mixing by increasing the core area of vortices and circulation along flow direction [31]. But this is not a desirable approach to enhance vortex strength or circulation at the cost of drag penalty. From these two aspects of PVGs and VGs, a new flow control device which is known as Double Sided Plasma Vortex Generator (DSPVG) as it has two exposed electrodes on its both sides, is proposed. This DSPVG has the advantages of device height (0.35δ) like submerged VGs as it placed normal to the controlled surfaces but zero yaw angle with flow direction to minimize the drag penalty. As it has dual exposed electrodes, hence plasma is created on both side that create two vortices and due to its placement in normal direction have better height advantages that embedded conventional PVGs. Due to device height and dual vortices on both sides, it is expected that the number of DSPVG is less required than conventional PVGs for flow control.

With a view to this, a winglet-type plasma actuator characterized the jet flow induced from the winglet by varying electrode position has been investigated at first. It was found that the most effective jet flow was induced if the exposed electrodes were located at the leading edge [32]. Considering this result, DSPVG is designed for the configuration which gives maximum induced flow. Due to design simplicity, this DSPVG is used as the vane of the vortex generator in a turbulent boundary layer flow. It induces flow from the tip to the hub on both sides of a vane. The induced flow is interacted with a boundary layer flow and produced a pair of stream-wise counter-rotating vortices. A yaw angle of the vane is zero against a free stream, and thus the drag penalty is expected to be low if the plasma is switched off.

METHOD

Diffuser and Measurement Methods

The experiment was conducted using an open-circuit wind tunnel (WIND TUNNEL: HD11-1 Honda dynamics, Japan; BLOWER: DV400,Sunada seisakusho, Japan) test section which was composed of a straight section and a diffuser section in Fluid Lab of TMU, Japan. The coordinate system of x, y, and z was defined as shown in Figure 1(a), and the coordinate origin was located at the inlet of the straight section. x and y correspond to the horizontal and vertical direction, respectively. The lengths of the straight and the diffuser section were 0.63m and 1.40m in the x-direction, respectively. The cross-section of the straight section was 0.2 m by 0.2 m. A tripping wire of 2 mm diameter was fixed at x = 50 mm in the straight section to develop a turbulent boundary layer. The slope of the diffuser section was inclined by 20° against the horizontal x-coordinate.

Streamwise location	x (mm)
1	450
2	550
3	630
4	660
5	690
6	730

Spanwise location	z (mm)
A	32
B	0
C	-32

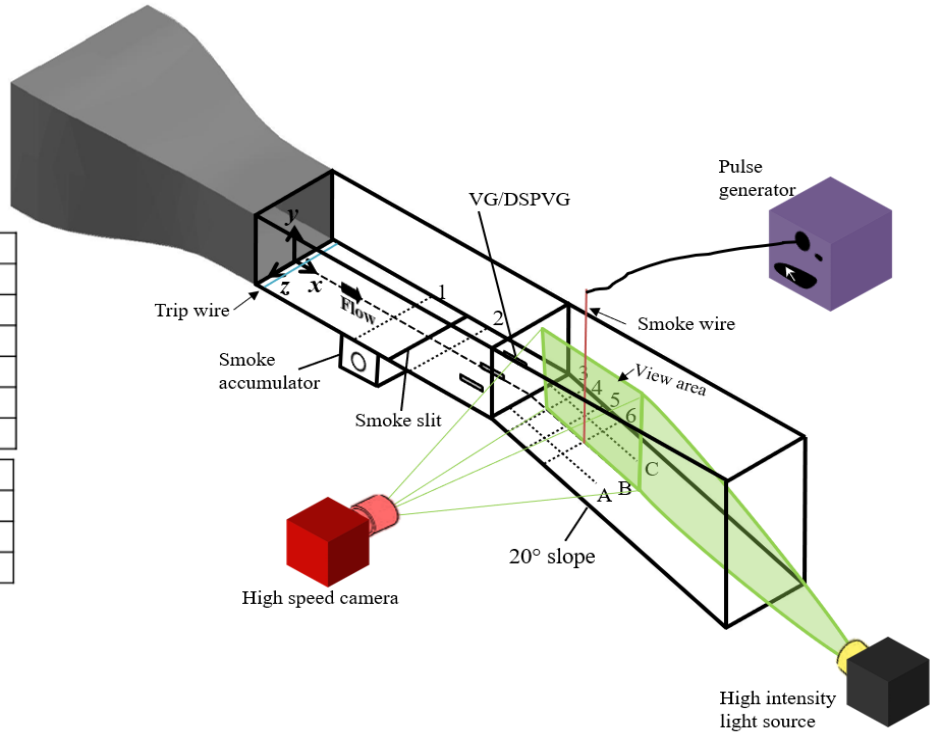

(a)

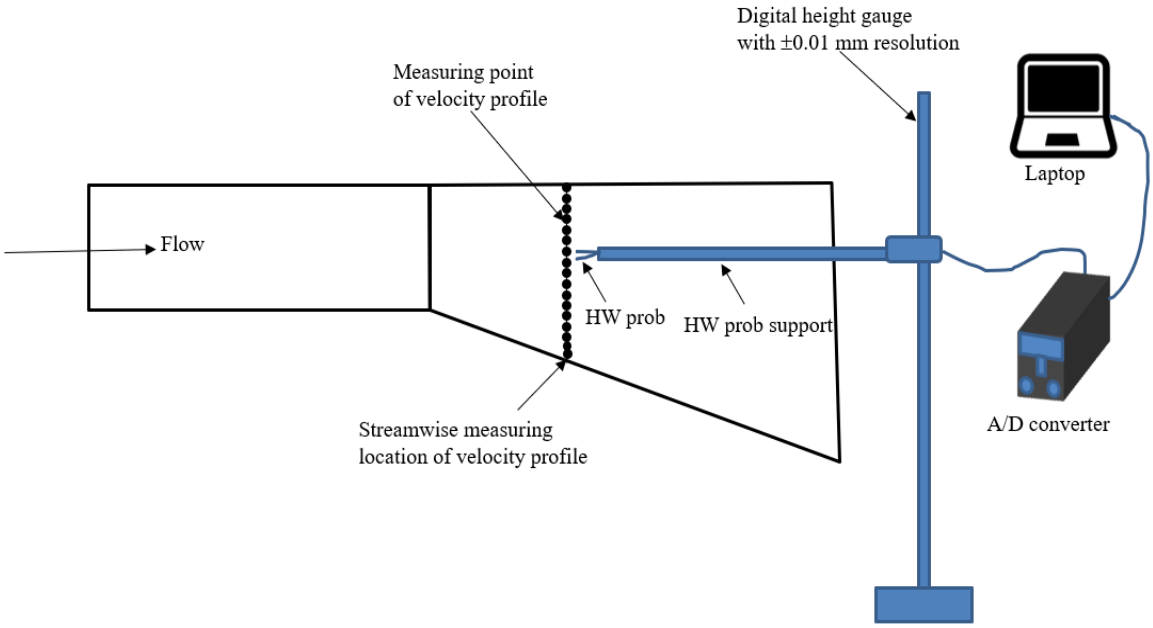

(b)

Figure 1. Schematic of a wind tunnel. (a) Measuring location with flow visualization setup, and (b) position of the hot-wire anemometer for the velocity measurement.

Flow separation on the slope was investigated using a hot-wire anemometer (CTA7100, Kanomax, Japan) and flow visualization. The overall flow behavior on the slope was visualized using a smoke sheet. The smoke was fed from a smoke generator (SLN-200, Nissho Electric Work Co. Ltd, Japan) to a smoke accumulator box, and then a smoke sheet was introduced along the wall surface from a wall slit. The boundary layer flow was visualized using time lines from a smoke wire of 0.2 mm diameter. The smoke wire was coated with Paraffin oil, and a pulse of high voltage was applied to the wire using a pulse generator (MS-405, Sugawara, Japan). The time lines of smoke were recorded with a high-speed video camera (MEMRICAM GX-1, NAC Image Technology, Japan).

The signal to the smoke wire triggered the start of the video camera recording with a time lag, which was controlled by a microcomputer (Uno, Arduino, Italy). Velocity was measured using a single hot-wire probe, which was installed in a traversing unit with digital scales. The output of the anemometer was recorded in a personal computer via an A/D processing unit (WE870, Yokogawa Electric Corp., Japan) with a sampling rate of 1900 1/s as shown in Figure 1(b). The total number of data sampled was 28000 for each point. When the DSPVG were used, spike-like noises appeared in the digitized data of the anemometer. These high frequency noises were removed by applying a high-cut filter of 200 Hz after sampling and this filter was applied to all anemometer data including the measurement data without the vane VGs and DSPVGs. Free stream velocity U_∞ was fixed to 4 m/s in this study (Re is 5.37E04, by considering the hydraulic diameter of the wind tunnel straight section as 0.2m). Hot-wire anemometer was calibrated by using ultrasonic velocimetry. The uncertainty was 1.25 % for the measurement of free stream velocity 4 m/s with a confidence level of 95%.

Conventional vortex generator and double-sided plasma vortex generator

Various reviews have been reported about several variations on the conventional vortex generators [5], [33]. As the present research deals with the effectiveness of DSPVG and its applicability with respect to conventional VG, hence the geometrical parameter of these VG/DSPVG should be considered wisely to achieve a better impact on flow control as it affects the performance of VG/DSPVG. In the present study, the yaw angle of the conventional vortex generator was fixed to 25°, as shown in Figure 2(c). The height and length of the conventional vortex generator were 7 mm and 28 mm, respectively. The same dimensions were used for the double-sided plasma vortex generator. The low freestream (of 4 m/s) velocity has been used due to the size limitation of DSPVG based on the cross-section of the wind tunnel. To be effective in higher velocity it is required either to increase the applied voltage on DSPVG (3.5 kV is used in this research) but the present size of DSPVG can't withstand with higher voltage (>3.5kV) or to increase the number of DSPVG's that requires more spanwise spacing in the wind tunnel. The present research is a series outcome of previous findings [32] in which the induced flow obtained by the same configuration of DSPVGs (double-sided plasma actuator was flush mounted from the surface and investigated at quiescent flow) is 1.2 m/s, so the ratio of induced flow/freestream velocity is 0.325 which is comparable with others [11-12], [21]. DSPVG's are placed parallel with flow direction i.e. the yaw angle was fixed to zero. This stream-wise alignment enables to minimize the drag penalty if the plasma is switched off. Three conventional VGs and DSPVGs were installed in the straight section. The DSPVG has an exposed electrode of 2.0 mm width on each side and a covered electrode of 5 mm width, as shown in Figure 2. The first investigation has been carried out on a winglet-type plasma actuator and results showed that if the exposed electrode was located at the leading edge, the highest velocity was achieved from the leading edge to the trailing edge [32]. Thus, this configuration of the exposed

electrode was applied to the double-sided plasma vortex generator. A Kapton film of 0.2 mm thickness was used as the dielectric material. The thickness of the DSPVG was 0.5 mm. The AC wave of ±4 kV amplitude and 5 kHz frequency were applied to the electrodes using a high voltage pulse generator (PSI-PG1040F, KI Tech., Japan).

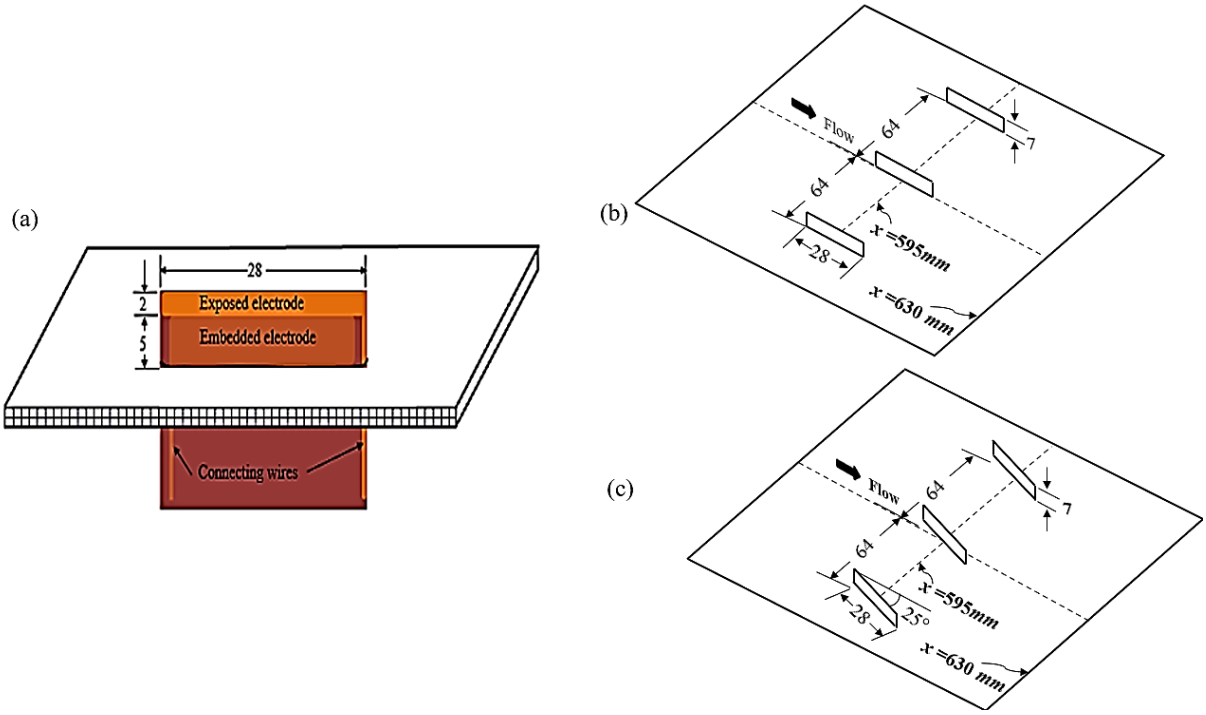

Figure 2. Dimensions and placement of DSPVG and conventional VG in wind tunnel. (a) Position of DSPVG and relative geometrical parameters (b) streamwise and spanwise placement of three DSPVGs (c) streamwise and spanwise placement of three conventional VGs.

Numerical Approach

In this article three conditions namely (i) flow without any VG/DSPVG (case-A) (ii) flow with vane vortex generator (case B) and (iii) flow with double-sided plasma vortex generator (case C) have been investigated experimentally and numerically. In case A, a fine mesh has been considered to capture better flow structure, especially in the separated region. k-ε is the simplest and popular turbulence model due to its easiness, lower computation expenses that can be used either by defining initial or boundary conditions. On the other hand k-ω SST combines the advantages of both k-ε and k-ω that works well with turbulent flow and capture the flow near the wall. Several researchers successfully applied k-ω SST in modeling flow in a diffuser, modeling of VG and plasma actuator enhanced flow due to its robustness and easy implementation [29-30], [34-35]. Both k-ε and k-ω SST model have been implemented for base line flow (case A). For case B and C, k-ω SST SST model is used. Flow domain and meshing for all cases have been shown in Figure 3. For Case C, the popular Suzen Model has been used for simulation, where the external body force (f_b) has been implemented to introduce the plasma effect by using user defined function (udf) to solve well known Navier-Stokes equation [36-37]. The equations were discretized using the finite volume method and velocity & pressure fields were coupled through the SIMPLE algorithm. The momentum and pressure equations were discretized using the second-order upwind scheme. Turbulence was modeled by using the first-order upwind scheme for VG and DSPVG's. For baseline case, finite volume method discretization is used with velocity and pressure fields were coupled through the PISO algorithm based on the recommendation of various researchers. The solution converge criteria were set to 10000 iteration steps with a tolerance limit equal to 1E-06. The convergence of the solution was also confirmed by monitoring the tendency of the residuals. There are total 2101115 nodes and 7120658 elements in the flow domain which is chosen for better computation result with optimal use of computing time as per grid independency test as shown in Figure 3(d). The corresponding solver setting has been shown in Table 1.

(a)

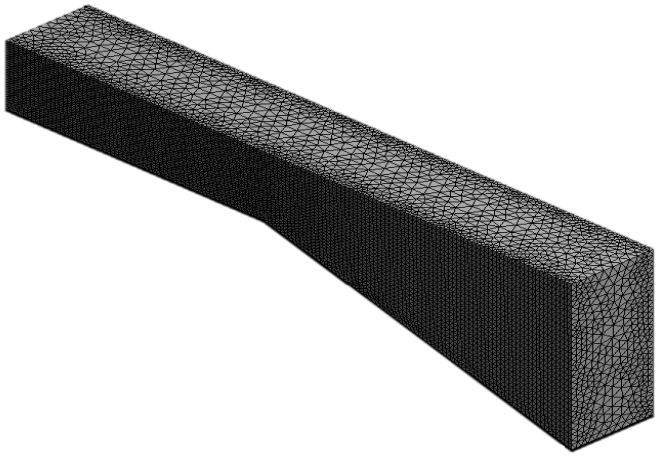

(b)

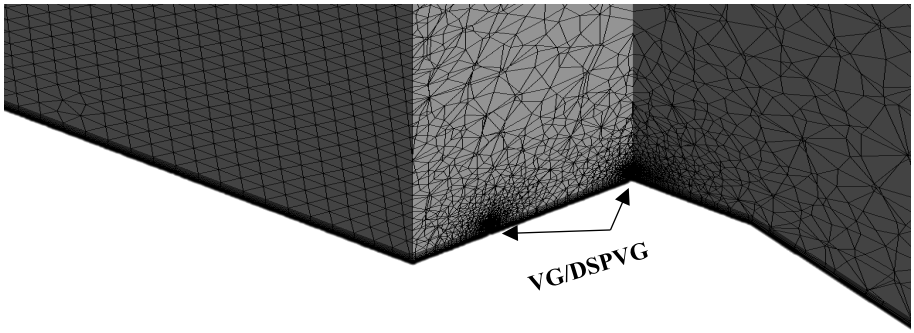

(c)

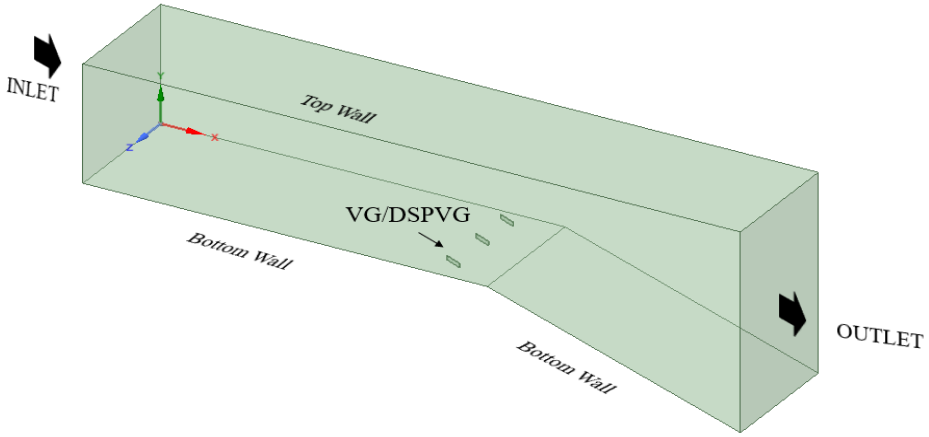

(d)

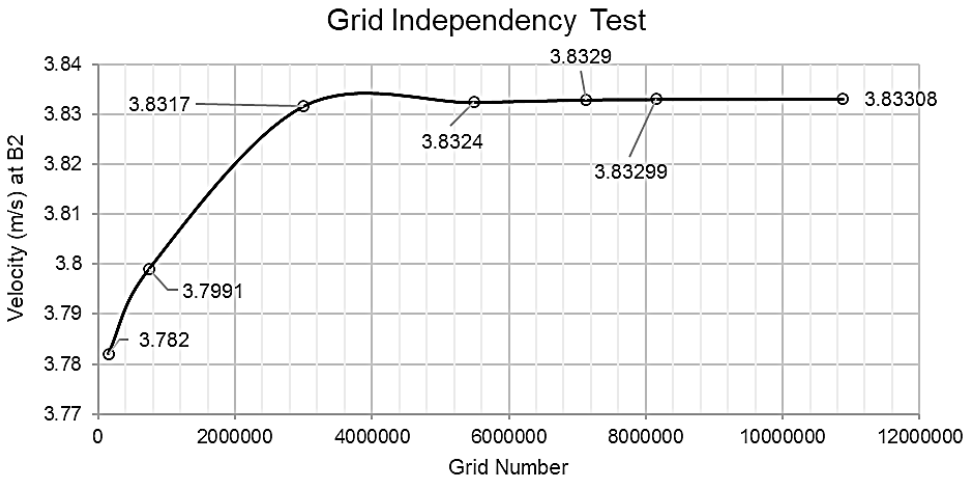

Figure 3. Details of meshing and flow domain. (a) Meshing of flow domain along streamwise direction, (b) meshing around VGs/DSPVGs in zoomed view, (c) flow domain and placement of DSPVG (angle with flow is 0°) and VGs (angle with flow is 25°) , and (d) grid independancy test.

Table 1. Boundary conditions and solver setup

	Case A (k-ε)	Case A (k-ω SST)	Case B and C
Model	k-ε (RNG) with enhance wall treatment	k-ω SST	k-ω SST
Inlet	Velocity inlet (4m/s)	Velocity inlet (4m/s)	Velocity inlet (4m/s)
Outlet	Pressure outlet	Pressure outlet	Pressure outlet
Bottom wall	No slip wall	No slip wall	No slip wall
VGs/DSPVGs	–	–	No slip wall and UDF for DSPVGs
Solution method	Pressure velocity coupling (PISO)	Pressure velocity coupling (PISO)	Pressure velocity coupling (SIMPLE)
Pressure	Second order	Second order	Second order
Momentum	Second order upwind	Second order upwind	Second order upwind
Turbulent KE	Second order upwind	Second order upwind	First order upwind
Turbulent dissipation rate	Second order upwind	Second order upwind	First order upwind

RESULTS AND DISCUSSION

Flow without VGs and DSPVGs

The stream wise velocity was measured in the straight section using a hot-wire anemometer. Figure 4 shows the profiles of the averaged velocity and the turbulent intensity along the span wise centerline B. The velocity profiles agreed with the turbulent velocity profile of a 1/7th law. The boundary layer thickness δ was defined as the height at which the velocity reached 0.99 U_∞. The thickness δ was 16mm at the location B1 (x = 450 mm), 19 mm at B2 (x = 550 mm), and 20 mm at B3 (x = 630 mm), respectively. The height of a typical low-profile vortex generator is 10 to 50% of a boundary layer thickness [5]. The height of the vortex generators used in this study is 35% of the boundary layer thickness and thus is comparable to the height of the low-profile vortex generators. The turbulent intensity in Figure 4(b) shows approximately the same profiles as that for the flat plate boundary layer flow [38]. Thus, the boundary layer flow produced in the straight section has characteristics that are approximately equivalent to those for the boundary layer flow without a pressure gradient.

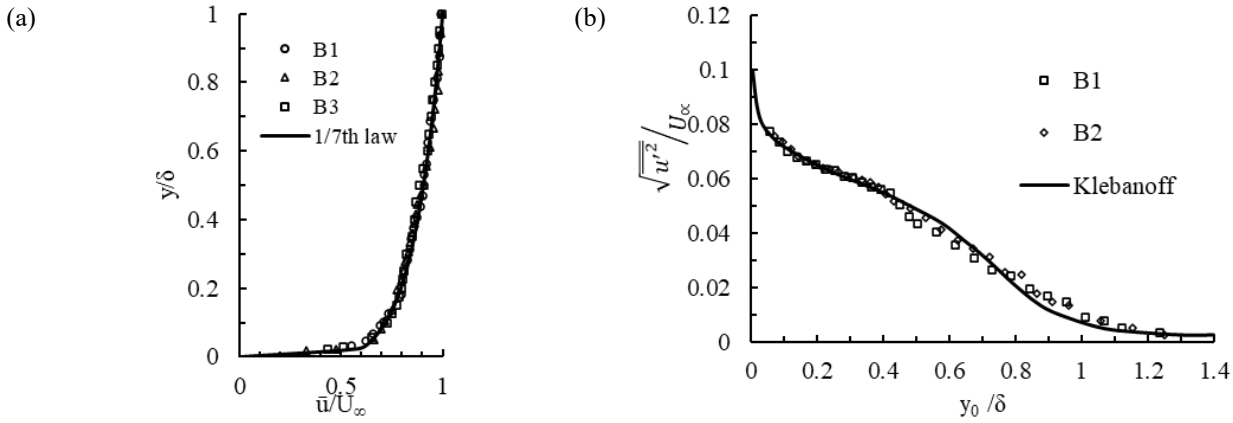

Figure 4. Time averaged profiles of velocity (a) and turbulent intensity (b) in the straight section.

A smoke sheet was fed to the diffuser section through a wall slit as shown in Figure 1(a), and the laterally form separation was observed at the diffuser section. The separation point was found to locate at x = 640 mm, which was 10 mm downstream from the start (x = 630 mm) of the diffuser section. Figure 5 was concocted from three pictures, which were obtained separately using a smoke wire. The picture was recorded using a high-speed video camera, the record of which was triggered by the signal to a smoke wire. y_0 is the vertical coordinate, the origin of which was shifted on the sloping wall. Three independent experiments were reduced to the same smoke pattern at each stream wise location, and thus the repeatability of the smoke pattern was confirmed. The averaged velocity profiles $|\overline{u}|$ were obtained using a hot-wire anemometer and plotted on the pictures of the smoke wire visualization, as shown in Figure 5. A hot-wire anemometer used here cannot discriminate the flow direction as it has single wire probe which detects the magnitude of flow, not direction. Thus, the agreement between the visualization and the anemometer was limited to region other than the reverse flow. The separated flow was observed at all three locations in Figure 5. The location B4 (at x = 660mm) was 20 mm downstream from the separation point x = 640 mm. Flow separation has also been observed from numerical analysis at x=640mm in k-ε and at x =642mm in k-ω SST model. Velocity contour and vector plot for each model is shown in Figure 6 and Figure 7 respectively.

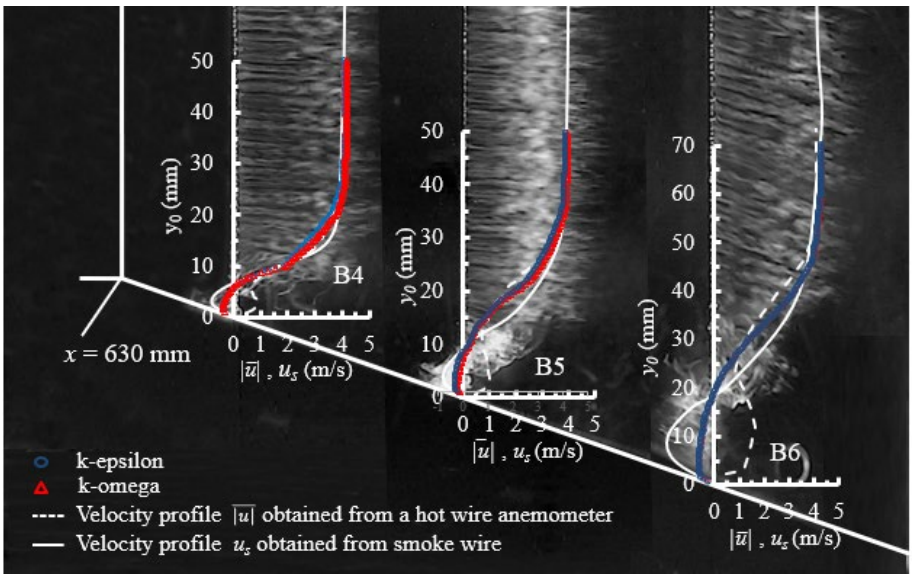

Figure 5. Flow separation without VGs/DSPVGs. The flow was visualized using a smoke wire. The pictures were taken at 10 ms after a high voltage pulse was applied to the smoke wire. Time averaged velocity profiles were obtained from a hot-wire anemometer. Simulated velocity profiles are also overlapped for corresponding measuring locations.

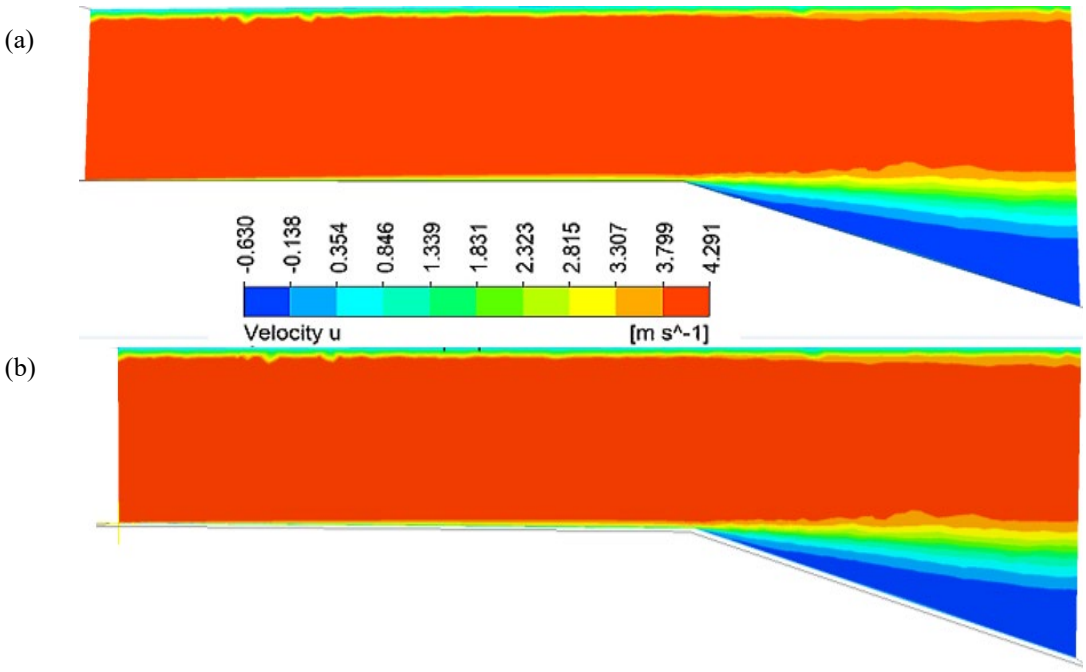

Figure 6. Flow velocity contour along B (centerline) clearly shows separated flow. (a) k-ε model. (b) k-ω SST model.

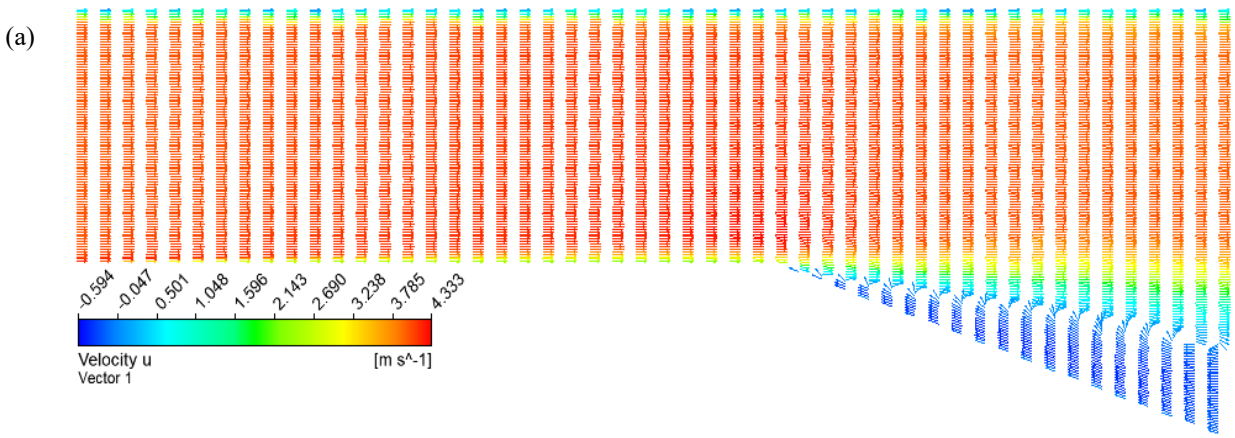

(b)

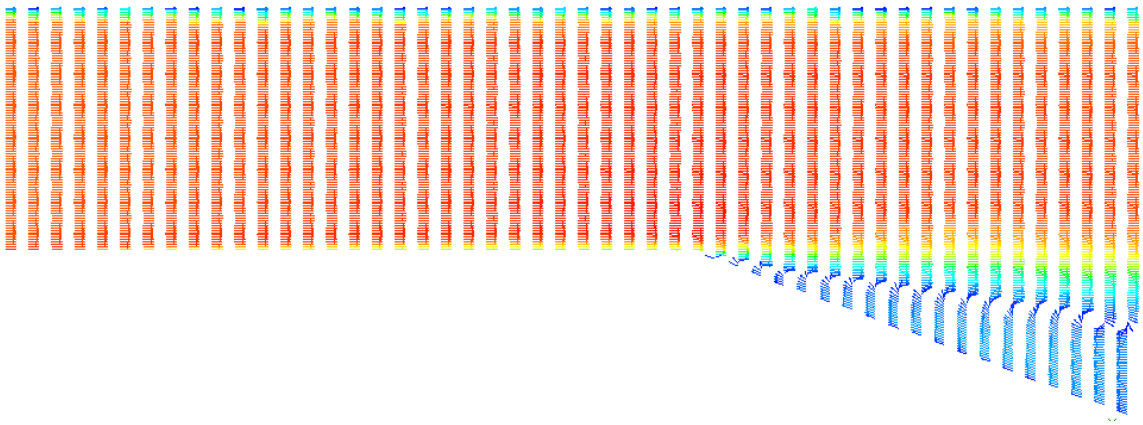

Figure 7. Velocity vector along B (centerline) clearly shows separated flow. (a) k-ε model. (b) k-ω SST model.

Separation Suppression by Conventional Vortex Generators and Double Sided Plasma Vortex Generators

As shown in Figure 8(a), the boundary layer flow was visualized on the slope using a smoke wire, the spanwise location of which was fixed to z = 0, in which the straight section was equipped with the conventional vortex generators. The streamwise locations of the smoke wire were B4, B5, and B6 along the center line B as shown in Figure 1. The smoke profiles indicated the elimination of separation on the slope. Using a hot-wire anemometer, the velocity profiles were measured at the three spanwise locations for each streamwise location and were plotted in Figure 8(b). The velocity profiles along line A shows deceleration compared with the other velocity profiles along lines B and C, because of the yaw angle of the conventional vortex generator, for which vortices also move downstream in an angular direction based on yaw angle. Although there were these spanwise differences among the velocity profiles of A, B, and C, these velocity profiles suggested similar elimination characteristics of separation at each streamwise location. The numerical investigation also complies with the experimental results. The conventional vane VGs suppress the separation in the measured location in the diffuser section. The velocity profile obtained from simulation has been compared with that of experimental results in Figure 8(a). Figure 9 represents the vector plot of VGs obtained from numerical simulation, in which it is revealed that the momentum added by the three vanes VGs have the ability to eliminate flow separation. A shape factor H is defined as the ratio of a displacement thickness to a momentum thickness in a boundary layer flow and is often used to predict flow separation. The boundary layer flow without a pressure gradient gives H = 1.4, and an increase in a positive pressure gradient increases H. In flow separation regions the value of H lies between 1.8 to 2.4 in a turbulent boundary layer flow [39]. This shape factor H was calculated using the velocity profile obtained from a hot-wire anemometer. The values of H were 1.7 at the location B4, 1.2 at B5, and 1.1 at B6, which were less than H (≅ 1.8 to 2.4) for a typical separation flow.

Figure 10(a) shows the results for the double-sided plasma vortex generators. The spanwise location of the smoke wire was fixed on the center line B. The smoke profiles indicated the elimination of separation similarly as the conventional vortex generators did. The results of a hot-wire anemometer were plotted in Figure 10(b). The results measured with the plasma switched off were also plotted to investigate the effect of plasma actuation. The velocity profiles obtained with the plasma switched on agreed approximately with the results of the smoke wire. The shape factors calculated were 1.5 at the location B4, 1.4 at B5, and 1.4 at B6, which were also less than H for a typical separation flow. Both the flow visualization and the hot-wire anemometer showed elimination of flow separation at the slope section by the plasma vortex generators. By contrast, the velocity profiles obtained with the plasma switched off agreed with the velocity profiles plotted in Figure 4 and showed the curves with inflection as in Figure 11. These inflectional curves are the characteristic velocity profiles of a reverse flow, because a hot-wire anemometer cannot discriminate the flow direction. These inflectional velocity profiles suggest that the switched-off plasma vortex generators do not have the effect of separation suppression, and thus the penalty of drag increase is also expected to be low. The simulted velocity profile of DSPVG has been shown in Figure 12 which reveals that the momentum added DSPVG suppress the flow separation. Although in all cases, the size of simulated flow domain is same; it is found that there is no separation of flow inside the measuring locarions by both DSPVGs and conventional VGs, but in comparison of Figure 9 and 12, it is found that flow is separated at 900mm (last measuring location, B6 is 730 mm) in case of VGs whereas no separated flow is observed in the whole domain in case of DSPVGs. That means, two vortices that are created by a single DSPVG on its both side, have much more ability to add momentum into the downstream than a conventional VG as it creates single vortex in one side only. That's why the present DSPVG provides better opportunity than conventional VGs by adding more momentum and as it is placed parallel with flow direction, there is no impact on flow condition in uncontrolled case i.e. switched off conditions. Moreover, DSPVGs have the height advantages than embeded plasma actuators or embedded PVGs that creates stronger vortices due to height advantages.

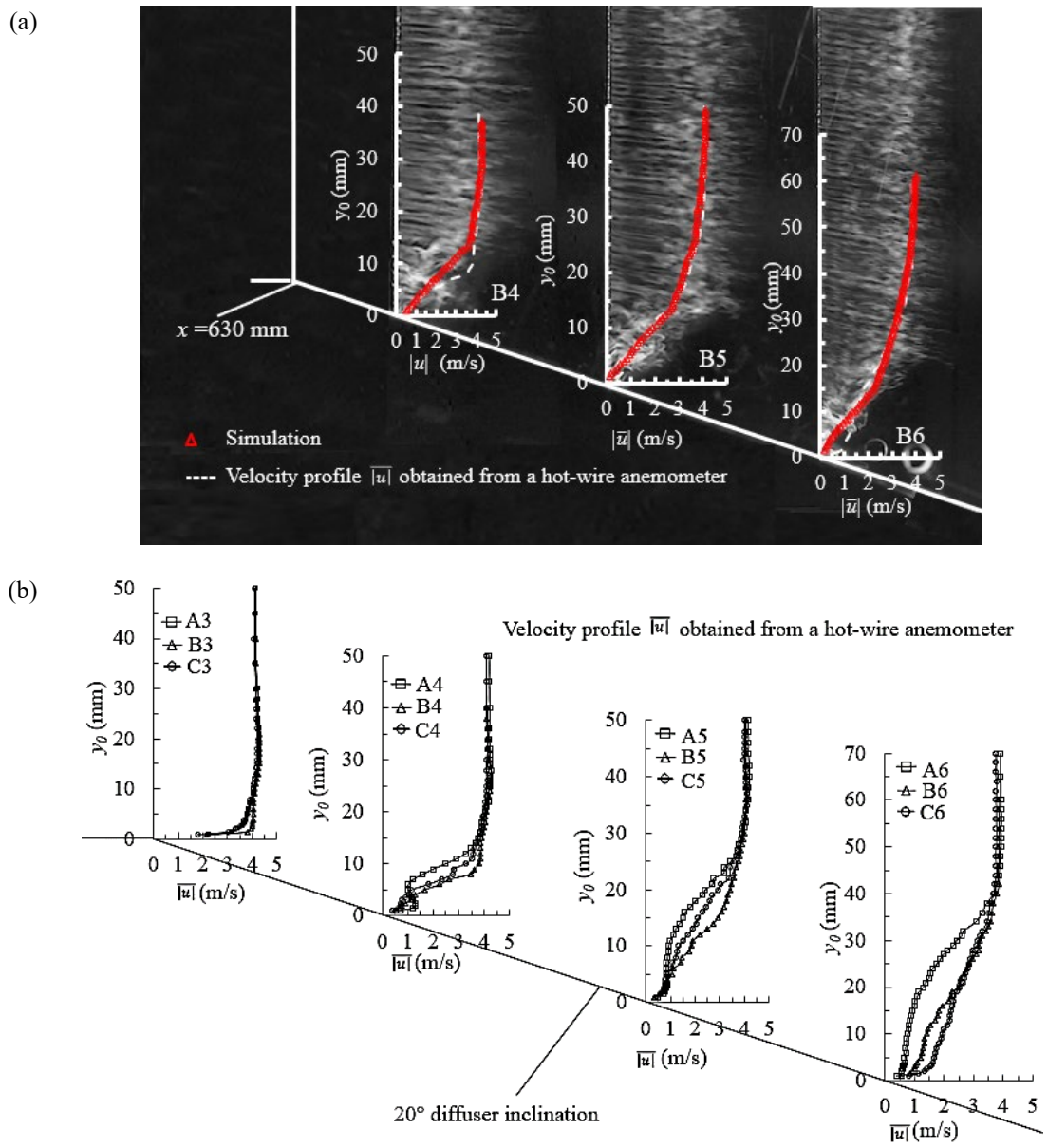

Figure 8. Separation elimination due to the conventional vortex generators. (a) Flow visualized using a smoke wire. Velocity profiles obtained from both hot wire and simulation shows reasonable agreement along B. (b) Time averaged velocity profiles obtained from a hot-wire anemometer. Although the results of (b) were dependent on the spanwise location, the results (b) along the center line B approximately agreed with the results (a) of the smoke wire and simulation.

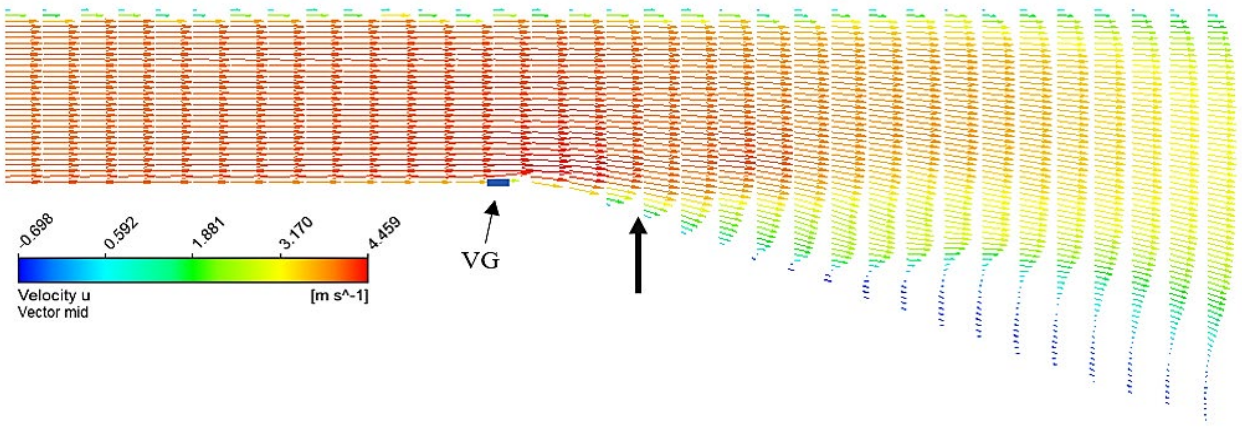

Figure 9. Numerical results of separation elimination by the conventional vortex generators. Velocity profiles along B shows the suppression of separation further downstream. Black arrow (↑) indicates the last measuring location (B6).

(a)

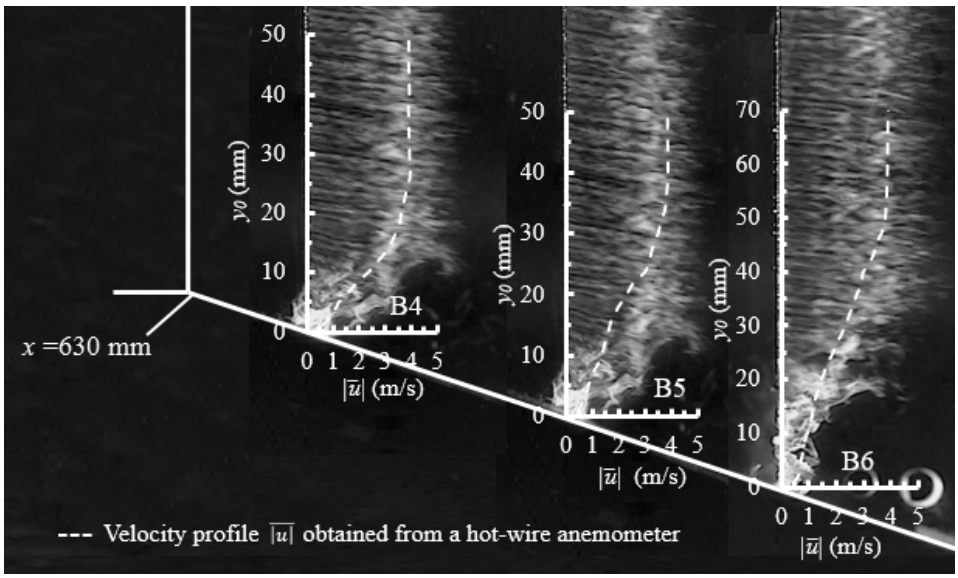

(b)

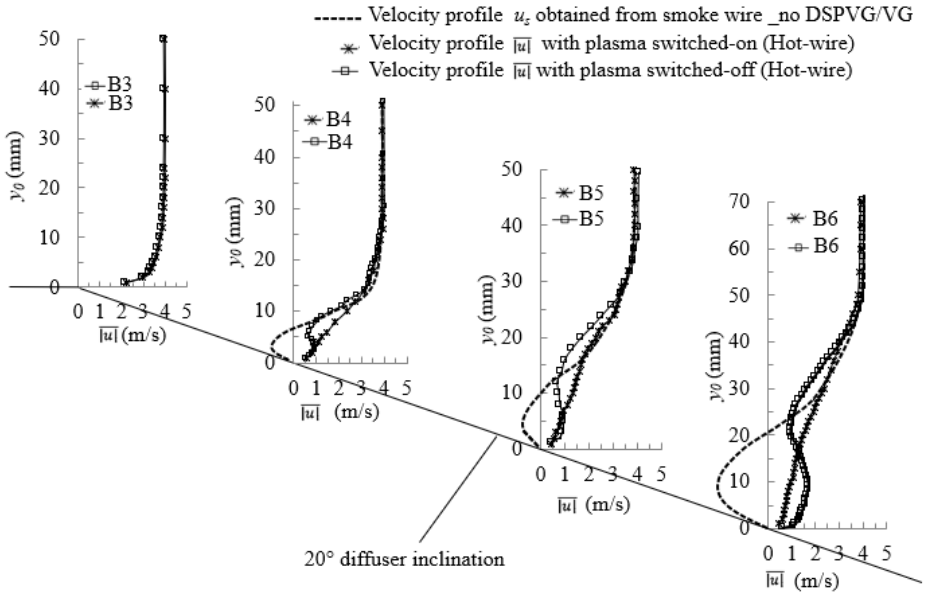

Figure 10. Separation elimination under the operation of double-sided plasma vortex generators. The spanwise location was the center line B. (a) Flow visualized using a smoke wire along the center line B. (b) Time averaged velocity profiles obtained from a hot-wire anemometer.

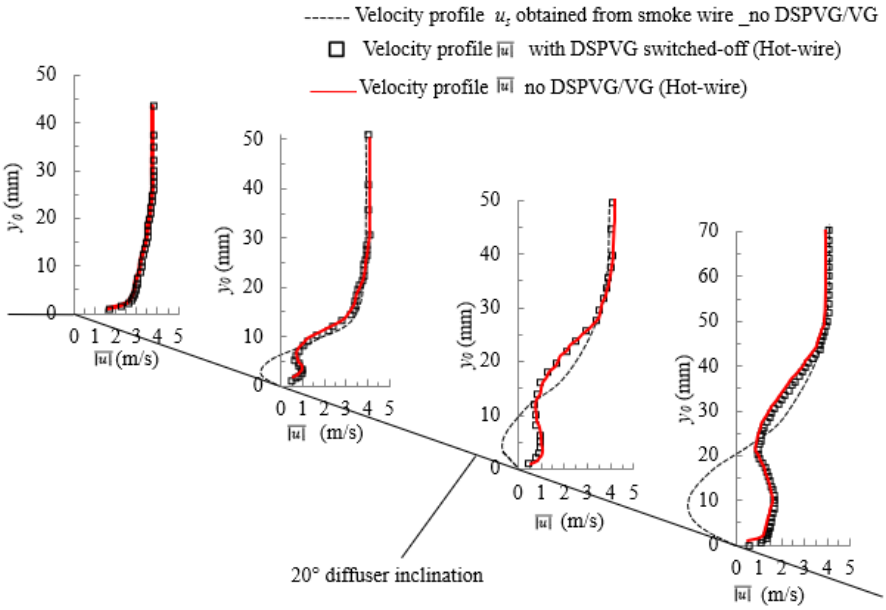

Figure 11. Time averaged velocity profiles without VG/DSPVG and DSPVG switched OFF condition.

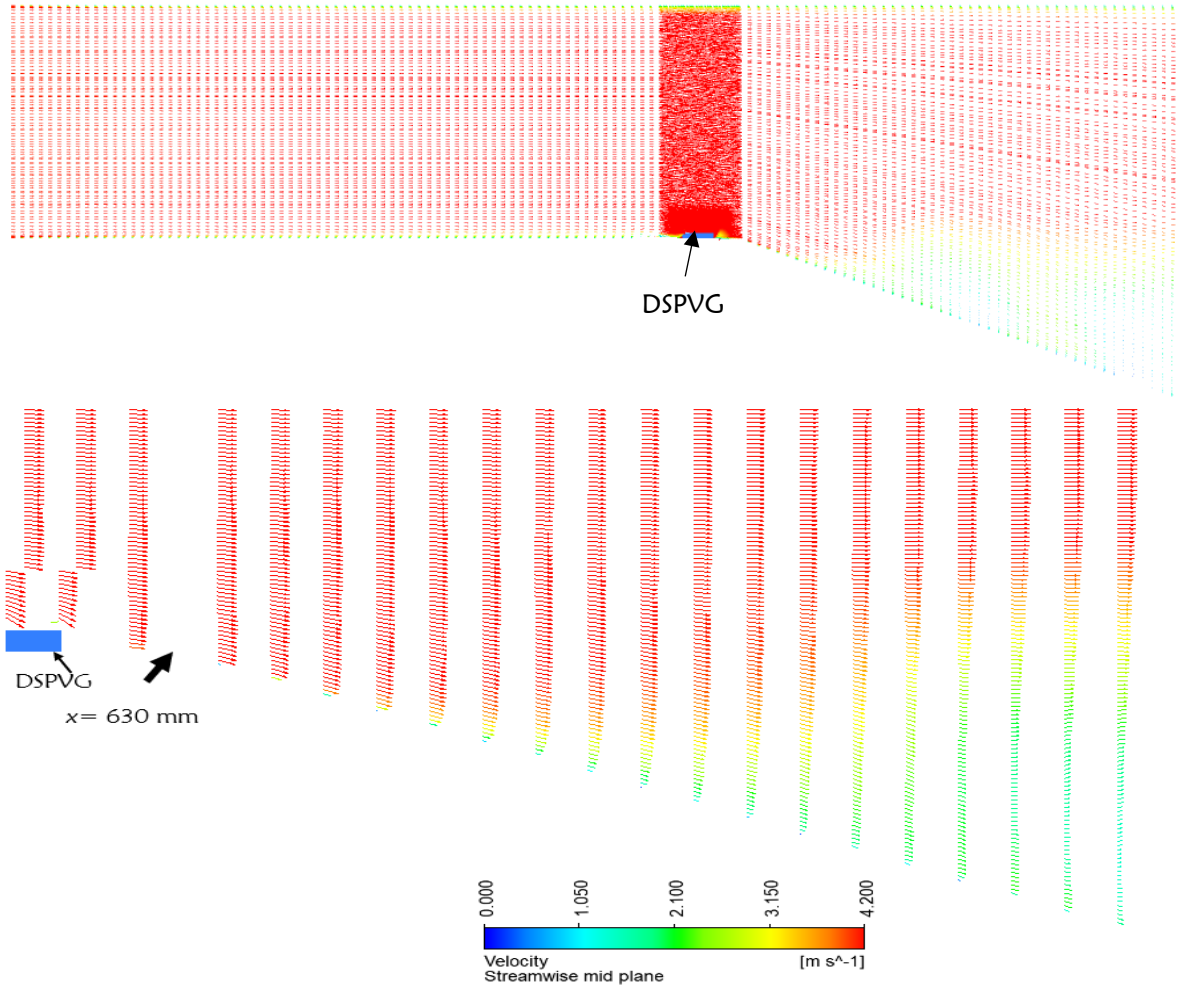

Figure 12. Numerical results of separation elimination by the double-sided plasma vortex generators. Velocity profiles along B show the suppression of separation further downstream. Vector of the whole domain is shown at the top and a cropped portion (DSPVG to end of flow domain in streamwise direction) is shown at the bottom.

The elimination effect of separation was also investigated through the turbulent intensity, which was obtained from the hot-wire data and was plotted in Figure 13. The turbulent intensities at the locations B3, B4, B5, and B6, are shown in Figure 13 (a) to (d) respectively. The flow without vortex generators showed slightly higher turbulence compared with the flows with the conventional and plasma vortex generators. With increasing x on the slope, the separated flow without

vortex generators shifted the height of the maximum turbulent intensity to the higher y_0, compared with the results for the conventional and plasma vortex generators. The turbulent intensities for the separation flow approximately agreed with the results obtained for the turbulent separation flow on a convex wall [40]. These results indicated that the DSPVGs had the effect of separation suppression similarly as the conventional vortex generators did but without the drag penalty.

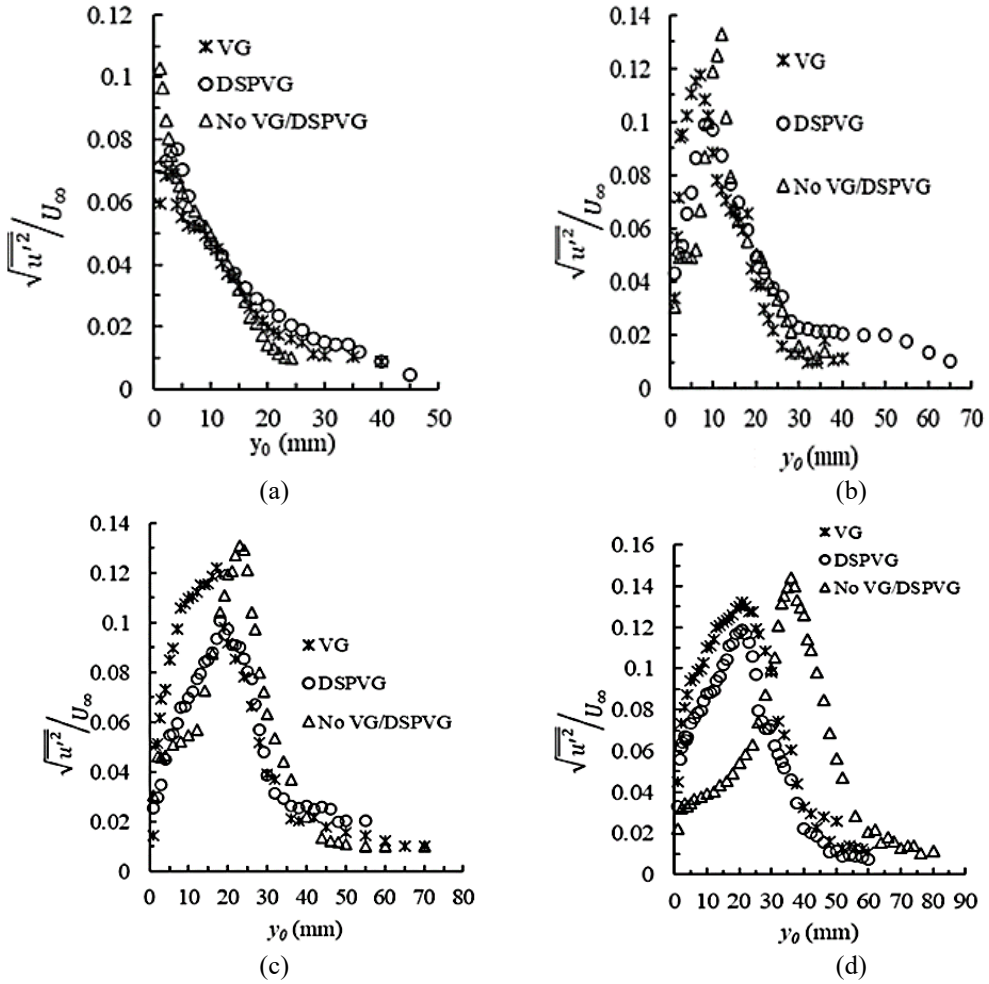

Figure 13. Profiles of turbulence intensity. The flow without VG/DSPVG shows a slightly higher peak of the turbulence intensity than those for the DSPVGs and conventional VGs. (a) at B3. (b) at B4. (c) at B5. (d) at B6.

CONCLUSION

A new vane-type double-sided plasma vortex generator (DSPVG) without a yaw angle has been investigated both experimentally and numerically to mitigate the drag penalty during the flow control. The computation results are in good agreement with experimental data in evaluating the effectiveness of both DSPVGs and VGs. The summary of findings are listed below:

i. The DSPVG is capable to eliminate the flow separation on the slope similarly as the conventional vortex generators did without drag penalty and has the advantage of device height to enhance mixing.
ii. The activity of DSPVG is controllable (Switch OFF and ON) as per requirement. The velocity profiles of DSPVG in switch-OFF condition give identical velocity profiles as that without any DSPVG/VG in the wind tunnel i.e. DSPVG has the ability to overcome device drag which is common in flow control by conventional VGs.
iii. Moreover, computational results showed that the momentum injection by dual vortices of DSPVGs is stronger than conventional VGs due to its single vortex.
iv. The DSPVGs have the advantages of device height, dual vortices on both sides and zero yaw angle along flow direction than conventional VGs and embedded PVGs which enables the DSPVG to provide more impact in separation control.
v. Turbulence intensity profiles from experiments give the same pattern for a regular convex wall.

ACKNOWLEDGEMENT

The experimental works have been carried out in the Fluid lab of TMU, Japan during the higher studies of the corresponding author.

REFERENCES

[1] G.B. Schubauer, and W.G. Spangenberg, "Forced mixing in boundary layers," *J. Fluid Mech.*, vol. 8, no. 1, pp. 10-32, 1960, doi: 10.1017/S0022112060000372.

[2] N. Titchener, and H. Babinsky, "A review of the use of vortex generators for mitigating shock-induced separation," *Shock Waves,* vol. 25, pp. 473–494, 2015, doi: 10.1007/s00193-015-0551-x .

[3] A.M. Jacobi, and R.K. Shah, "Heat transfer surface enhancement through the use of longitudinal vortices: a review of recent progress," *Exp. Therm. Fluid Sci*., vol. 11, no. 3, pp. 295–309, 1995, doi: 10.1016/0894-1777(95)00066-U.

[4] A.N.M.M.I. Mukut, and M.Z. Abedin, "Review on aerodynamic drag reduction of vehicles," *International Journal of Engineering Materials and Manufacture*, vol. 4, no. 1, pp. 1-14, 2019, doi: 10.26776/ijemm.04.01.2019.01.

[5] J.C. Lin, "Review of research on low-profile vortex generators to control boundary-layer separation," *Prog. Aerosp. Sci.,* vol. 38, no. 4-5, pp. 389-420, 2002, doi: 10.1016/S0376-0421(02)00010-6.

[6] G. Linyue, Z. Hui, L. Yongqian, and H. Shuang, "Effects of vortex generators on a blunt trailing-edge airfoil for wind turbines. *Renew. Energy*, vol. 76, pp. 303-311, 2015, doi: 10.1016/j.renene.2014.11.043.

[7] E.J. Sandeep, Z. Liwei, and K.L. Frank, "Numerical study of drag reduction by conventional and micro vortex generators," In AIAA 2021-2857. AIAA Aviation 2021 Forum, August 2021, doi: 10.2514/6.2021-2857.

[8] T.N. Jukes, and K.S. Choi, "Dielectric-barrier-discharge vortex generators: characterization and optimization for flow separation control," *Exp. Fluids,* vol. 52, pp. 329-345, 2012, doi: 10.1007/s00348-011-1213-0.

[9] J. Julian, C-C Wang, and M-J Chern, "Effect of plasma actuator in boundary layer on flat plate model with turbulent promoter," *Proc. Inst. Mech. Eng. G: J. Aerosp. Eng.,* vol. 232, no. 16, pp. 3001-3010, 2018, doi:10.1177/0954410017727301.

[10] S. Nima, R.K. Matthias, and H. Ardeshir, "Control of a swept-wing boundary layer using ring-type plasma actuators," *J. Fluid Mech.*, vol. 844, no. 10, pp. 36–60, 2018, doi: 10.1017/jfm.2018.195.

[11] J.A. Vernet, R. Örlü, and P.H. Alfredsson, "Flow separation control behind a cylindrical bump using dielectric-barrier-discharge vortex generator plasma actuators," *J. Fluid Mech.*, vol. 835, pp. 852–879, 2018, doi:10.1017/jfm.2017.773.

[12] T.N. Jukes, and K.S. Choi, "On the formation of streamwise vortices by plasma vortex generators," *J. Fluid Sci. Technol.* vol. 733, pp. 370-393, 2013, doi: 10.1017/jfm.2013.418.

[13] F.F. Rodrigues, J.C. Pascoa, and M. Trancossi, "Analysis of innovative plasma actuator geometries for boundary layer control," In Proceedings of the ASME 2016 International Mechanical Engineering Congress and Exposition IMECE2016 Phoenix, AZ, 2016, pp.1-10, doi: 10.1115/IMECE2016-66495.

[14] M. Blajan, D. Nonaka, J. Kristof, Shimizu, and Kazuo, "Study of Induced EHD Flow by Microplasma Vortex Generator," *IEEE Transactions on Plasma Science*, vol. 47, no.12, pp. 5345–5354, 2019, doi: 10.1109/TPS.2019.2952166.

[15] T.N. Jukes, T. Segawa, and H. Furutani, "Flow control on a NACA 4418 using dielectric-barrier-discharge vortex generators," *AIAA Journal*, vol. 51, pp. 452-464, 2013, doi: 10.2514/1.J051852.

[16] X. Zhang *et al.*, "Turbulent boundary layer separation control using plasma actuator at Reynolds number 2000000," *Chinese J. Aeronaut.*, vol. 29, pp. 1237-1246, 2016, doi: 10.1016/j.cja.2016.08.006.

[17] H. Akbıyık, and H. Yavuz, "Active flow control with dbd plasma vortex generators around a NACA 2415 airfoil," *Journal of Institue of Science and Technology*, vol. 37, no. 2, pp. 296-305, 2021.

[18] S. Im, M.S. Bak, M.G. Mungal, and M.A. Cappelli, "Dielectric barrier discharge-induced vortex generation with discharge-actuated boundary layer bleed," *IEEE Tran.s Plasma Sci.,* vol. 41, no. 12, pp. 3345-3253, 2013, doi: 10.1109/TPS.2013.2278027.

[19] H. Gejima *et al.*, "Suppression of vortex shedding from a pantograph head using vortex-generator plasma actuators," *J. Fluid Sci. Technol.*, vol. 10, pp. 1-12, 2015, doi: 10.1299/jfst.2015jfst0006.

[20] J.A. Vernet *et al.*, "Plasma streamwise vortex generators for flow separation control on trucks," *Flow Turbul. Combust.*, vol. 100, pp. 1101–1109, 2018, doi: 10.1007/s10494-018-9891-9.

[21] X.Q. Cheng *et al.*, "Flat plate drag reduction using plasma-generated streamwise vortices," *J. Fluid Mech.*, vol. 918, pp. 1-37, 2021, doi:10.1017/jfm.2021.311.

[22] F.O. Thomas *et al.*, "Turbulent drag reduction using pulsed-DC plasma actuation," *J. Phys. D: Appl. Phys.*, 52 (434001). 2019, doi:10.1088/1361-6463/ab3388.

[23] T.C. Corke and F.O. Thomas, "Active and passive turbulent boundary-layer drag reduction," *AIAA Journal*, pp. 1–13. 2018, doi:10.2514/1.J056949.

[24] O. Mahfoze, and S. Laizet, "Skin-friction drag reduction in a channel flow with streamwise-aligned plasma actuators," *Int. J. Heat Fluid Flow*, vol. 66, pp. 83-94, 2017, doi: 10.1016/j.ijheatfluidflow.2017.05.013.

[25] A. Ghayour, and M. Mani, "Experimental investigation of plasma vortex generator in flow control," *Aircr. Eng. Aerosp.*, vol. 92, no. 3, pp. 376-385, 2018, doi: 10.1108/AEAT-07-2018-0194.

[26] K.S. Choi *et al.*, "Plasma virtual actuators for flow control," *J. Flow Control Meas. Visual.*, vol. 3, no. 1, pp. 22-34, 2015, doi: 10.4236/jfcmv.2015.31003.

[27] X-k Li *et al.*, "Analysis of the effect of vortex generator spacing on boundary layer flow separation control," *Appl. Sci.*. vol. 9(24), pp. 1-22, 2019, doi: 10.3390/app9245495.

[28] D. Baldacchino *et al.*, "Experimental parameter study for passive vortex generators on a 30% thick airfoil," *Wind Energy*, vol. 21, pp. 745– 765, 2018, doi:10.1002/we.2191.

[29] Y. Yan, E. Avital, J. Williams, and J. Cui, "CFD analysis for the performance of micro-vortex generator on aerofoil and vertical axis turbine," *J. Renew. Sustain. Energy*, vol. 11(043302), pp. 1-24, 2019, doi: 10.1063/1.5110422.

[30] A.P. Heffron, J.J. Williams, and E. Avital, "Numerical and experimental study of microvortex generators," *J. Aircr.*, pp. 1–11, 2018, doi:10.2514/1.C034550.

[31] X. Li, K. Yang, and X. Wang, "Experimental and numerical analysis of the effect of vortex generator height on vortex characteristics and airfoil aerodynamic performance," *Energies,* vol. 12, no. 5, pp. 1-19, 2019, doi: 10.3390/en12050959.

[32] A.N.M.M.I. Mukut, H. Mizunuma, H. Obara, and T. Segawa, "Flow characteristics induced by winglet-type plasma actuators," *J. Fluid Sci. Technol.,* vol. 8, no. 3, pp. 396-406, 2013, doi: 10.1299/jfst.8.396.

[33] P.K. Chang, *Control of flow separation*. Hemisphere Publishing Corporation, McGraw-Hill Book Company, 1976.

[34] C. He, "Plasma Slats and Flaps: An Application of Plasma Actuators for Hingeless Aerodynamic Control," Ph.D thesis, University of Notre Dame, USA, 2010.
[35] M.A. Abd Halim, N.A.R. Nik Mohd, M.N. Mohd Nasir, and M.N. Dahalan, "The evaluation of k-ε and k-ω turbulence models in modelling flows and performance of s-shaped diffuser," *Int. J. Automot. Mech. Eng.*, vol. 2, pp. 5161-5178, 2018, doi: 10.15282/ijame.15.2.2018.2.0399.
[36] Y.B Suzen, P.G. Huang, J.D. Jacob, and D.E. Ashpis, "Numerical simulation of plasma based flow control applications, " In 35th Fluid Dynamics Conference and Exhibit AIAA 2005-4633, Toronto, Ontario, Canada; 06-09 June 2005, doi: 10.2514/6.2005-4633
[37] Y.B Suzen, and P.G. Huang, "Simulations of flow separation control using plasma actuators," In 44th AIAA Aerospace Sciences Meeting and Exhibition, AIAA 2006-877, Reno, Nevada; 9 - 12 January 2006, doi: 10.2514/6.2006-877.
[38] P.S. Klebanoff, Characteristics of turbulence in boundary layer with zero pressure gradient. NACA Report 1247, 1955.
[39] H. Schlichting, *Boundary layer theory*. 6th Ed. McGRAW-HILL. 1968, p.639. doi: 10.1007/978-3-662-52919-5.
[40] Q. Wei, and H. Sato, "An experimental study of the mechanism of intermittent separation of a turbulent boundary layer," *J. Fluid Mech.*, vol. 143, pp. 153-172, 1984, doi: 10.1017/S0022112084001294.